Radium isotopes as a tracer of sediment-water column exchange in the North Sea

Burt, W. J.; Thomas, H.; Paetsch, J.; Omar, A. M.; Schrum, C.; Daewel, U.; Brenner, H.; de Baar, H. J. W.

Published in:
Global Biogeochemical Cycles

DOI:
10.1002/2014GB004825

Publication date:
2014

AGU PUBLICATIONS

Global Biogeochemical Cycles

RESEARCH ARTICLE
10.1002/2014GB004825

Radium isotopes as a tracer of sediment-water column exchange in the North Sea

W. J. Burt[1], H. Thomas[1], J. Pätsch[2], A. M. Omar[3,4], C. Schrum[5,6], U. Daewel[5,6], H. Brenner[7], and H. J. W. de Baar[8]

[1]Department of Oceanography, Dalhousie University, Halifax, Nova Scotia, Canada, [2]Institute of Oceanography, University of Hamburg, Hamburg, Germany, [3]Uni Research Climate, Norway, [4]Geophysical Institute, University of Bergen, Norway, [5]Geophysical Institute, University of Bergen and Hjort Centre for Marine Ecosystem Dynamics, Bergen, Norway, [6]Nansen Environmental and Remote Sensing Center and Hjort Center for Marine Ecosystem Dynamics, Bergen, Norway, [7]Department of Ecosystem Studies, Royal Netherlands Institute for Sea Research, Yerseke, Netherlands, [8]Royal Netherlands Institute for Sea Research (NIOZ), Texel, Netherlands

Key Points:
- Ra distributions indicate dominant sedimentary Ra source
- Sediment characteristics and turbulence regime regulate benthic Ra fluxes
- Ra distributions are reproduced using observed fluxes in a passive tracer model

Correspondence to:
W. J. Burt,
willburt@dal.ca

Citation:
Burt, W. J., H. Thomas, J. Pätsch, A. M. Omar, C. Schrum, U. Daewel, H. Brenner, and H. J. W. de Baar (2014), Radium isotopes as a tracer of sediment-water column exchange in the North Sea, *Global Biogeochem. Cycles*, *28*, 786–804, doi:10.1002/2014GB004825.

Received 5 FEB 2014
Accepted 16 JUL 2014
Accepted article online 18 JUL 2014
Published online 12 AUG 2014

Abstract Sediment-water column exchange plays an important role in coastal biogeochemistry. We utilize short-lived radium isotopes (^{224}Ra and ^{223}Ra) to understand and quantify the dominant processes governing sediment-water column exchange throughout the North Sea. Our comprehensive survey, conducted in September 2011, represents the first of its kind conducted in the North Sea. We find that two main sources regulate surface Ra distributions: minor coastal input from rivers and shallow mudflats and North Sea sediments as the dominant source. Pore waters show 100-fold larger activities than the water column. North Sea sediment characteristics such as porosity and mean grain size, as well as turbulence at the sediment-water interface, are the dominant factors contributing to variability of Ra efflux. Ra inventory and mass balance approaches consistently yield high benthic Ra effluxes in the southern North Sea, driven by strong tidal and wind mixing, which in turn cause high sediment irrigation rates. These results exceed incubation-based Ra flux estimates and the majority of previously reported Ra flux estimates for other regions. Ra-based estimates of benthic alkalinity fluxes compare well to observed values, and the high rates of Ra efflux imply a potentially significant exchange of other products of sedimentary reactions, including carbon and nutrient species. Passive tracer simulations lend strong support to the Ra source attribution and imply seasonal variation in the surface water Ra distribution depending on stratification conditions.

1. Introduction

The cycling of material between the water column and the underlying sediments can play an important role in biogeochemical cycles. This is especially true in coastal and shelf sea regions like the North Sea, where high sedimentation rates generate intense chemical cycling within the sediments. As seawater enters and flows through permeable sediments, it becomes chemically enriched in the products of numerous diagenetic reactions. The sediment pore waters, rich in carbon, nutrients, and metals, are then transported through the sediment-water interface by a variety of transport mechanisms.

Diffusion and bioturbation are important processes in fine-grained cohesive sediments. However, exchange in more permeable sandy sediment, which is the predominant sediment type both in the North Sea, and globally in shelf seas, is often dominated by advective flows [*Aller*, 1980; *Janssen et al*., 2005a]. Advective transport, termed here as sediment irrigation, is driven mainly by pressure gradients as boundary currents or gravity waves flow over sediment topography [*Precht and Huettel*, 2003]. In subtidal regions, sediment irrigation can also occur via tidal flooding or groundwater pumping [*Rusch and Huettel*, 2000].

Strong tidal and wind-induced mixing of relatively shallow waters can bring sediments into contact with surface waters, allowing direct and rapid exchanges between the sedimentary, marine, and atmospheric reservoirs. An important consequence of this is that sediment-water exchange of recycled nutrients also plays a significant role in nutrient and carbon cycling of the North Sea [*Luff and Moll*, 2004]. In general, burial of organic material is considered negligible throughout the majority of the North Sea [*de Haas et al*., 2002; *Pätsch and Kühn*, 2008] meaning that the estimated 17–45% of North Sea primary production that is degraded within sediments [*van Duyl and Kop*, 1994] is almost entirely released back into the water column. In this type of coupled system, sedimentary reactions such as denitrification and sulfate reduction

can lead to the release of excess alkalinity from sediments, which has an effect on the buffering capacity of coastal surface waters [*Thomas et al*., 2009]. This leads to an alteration in the ability of surface waters to take up atmospheric CO_2.

Marine sediments are also enriched in thorium (Th), which is strongly adsorbed to particle surfaces. Alpha decay of Th continuously generates radium (Ra) isotopes that, due to their lower affinity to particles, build up in the pore waters. Once transported through the sediment-water interface, Ra is dispersed away from its source, and its activity decreases due to decay. In coastal systems, dissolved Ra enters both laterally across the land-ocean boundary (i.e., from the subterranean estuary or from rivers) and vertically across the sediment-water column boundary. Knowledge of the distinct source regions along with relatively simple behavior, make Ra isotopes powerful tracers for quantifying rates of sediment-water column exchange. Another benefit of the Ra suite of tracers is their largely varying half-lives (3.7 days to 1600 years), which allow for interpretation of processes that occur over multiple spatial and temporal scales. For example, at regions far offshore (>100 km), the coastal signal of the shorter-lived Ra species, ^{224}Ra ($t_{1/2}$ = 3.7 d) and ^{223}Ra ($t_{1/2}$ = 11.4 d), is likely negligible, meaning any detectable activities must come from relatively recent interaction with bottom sediments [e.g., *Burt et al*., 2013b].

Although the North Sea is one of the world's most heavily studied coastal regions, many uncertainties still exist regarding the effects of different boundary exchanges on the biogeochemistry of the system. For example, recent studies have shown that the combination of sediment-water column exchange within the shallow mudflats of the adjacent Wadden Sea, and subsequent lateral (i.e., land-ocean) exchange through tidal channels are an important source of dissolved nutrients, trace metals, and alkalinity to the North Sea [*Thomas et al*., 2009; *Moore et al*., 2011; *Winde et al*., 2014] and directly influence atmospheric CO_2 fluxes [*Omar et al*., 2010]. Numerous studies have closely examined aspects of sediment-water column exchange in the Wadden Sea [e.g., *Beck et al*., 2008; *Moore et al*., 2011], yet direct observations of this exchange in the open North Sea are lacking. Prior studies are limited to estimates of diffusive nutrient fluxes in different regions of the southern North Sea using pore water profiles and sediment incubations [*Rutgers van der Loeff*, 1980; *van Raaphorst et al*., 1990, 1992]. Current numerical modeling studies in the North Sea have concluded that better representation of these exchanges are needed to improve the modeled biogeochemical cycling in the coastal regions [*Daewel and Schrum*, 2013], and adding complexity to sediment modules remains critical to better representing the North Sea biogeochemistry as a whole.

To date, Ra studies in the North Sea region have been very limited. *Shaw* [2003] first discussed the potential utility of Ra isotopes in quantifying the transport of chemically enriched waters from the Wadden Sea into the North Sea. *Schmidt et al*. [2010] provided the first published Ra measurements in the German Bight of the North Sea, as well as insight and motivation toward future Ra studies. Finally, an extensive study by *Moore et al*. [2011] created a Ra mass balance to successfully quantify the discharge of chemically enriched pore waters into the Wadden Sea as well as the release of Ra and other dissolved substances into the North Sea.

In this paper, rates of sediment-water column exchange in the North Sea are examined. We employ results from a basin-wide Ra isotope survey of the North Sea, conducted in the summer of 2011. Horizontal and vertical water column distributions are used to identify key Ra sources to the North Sea, and together with results from sediment incubations, benthic Ra fluxes are quantified using a variety of independent approaches. The important mechanisms of sediment-water column exchange in the North Sea are identified, as are the dominant controls on the observed Ra fluxes. Estimates of pore water Ra facilitate the quantification of the volume of water exchanged through the sediment-water interface, which can then be used to estimate benthic alkalinity fluxes. Finally, the use of a 3-D hydrodynamic model allows us to simulate the distributions of Ra as a passive tracer, which provides insight into Ra source attribution and seasonal variations of Ra distributions in the North Sea. Overall, the results presented highlight the utility of Ra isotopes for use as a tracer of sediment-water column exchange in coastal systems.

2. Study Area

The North Sea (Figure 1), located on the NW European shelf, can be separated into two distinct regions: The shallower (<50 m depth) southern North Sea (SNS) is strongly influenced by tidal and wind-induced mixing with part of it well mixed throughout the year. The deeper northern North Sea (NNS) is

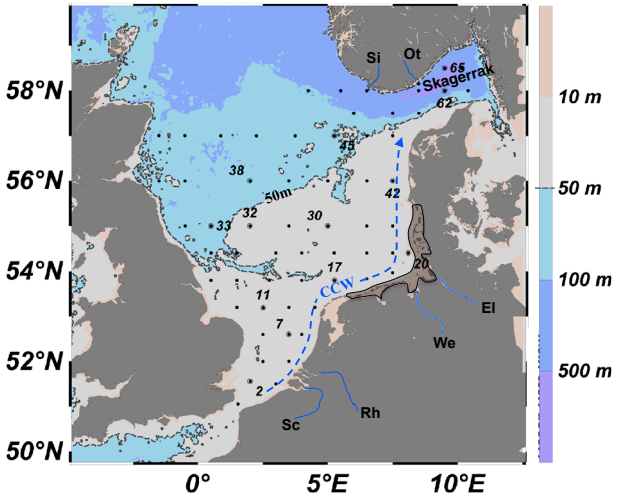

Figure 1. Map of North Sea with stations sampled for Ra during the 2011 cruise (black dots). Stations with any additional Ra sampling (deep profile, incubation, or pore water) are labeled with the station number. The 50 m contour (dashed line) roughly traces the border between well-mixed stations to the south and stratified stations to the north during the time of observations. The Wadden Sea is outlined in the black shaded box, and the general circulation path of the continental coastal waters (CCW) is shown. Relevant rivers are also labeled: Sc = Scheldt, Rh = Rhine, We = Weser, El = Elbe, Ot = Otra, and Si = Sira.

seasonally stratified [*Lee*, 1980]. For this study, the border between these two regions can be drawn almost flawlessly using the 50 m depth contour (Figure 1, black dashed line).

Exchange with the North Atlantic Ocean at the open northern boundary dominates the volume transport. The general circulation pattern is a cyclonic flow with inflow through the Shetland Channel and Faire Island Channel on the western side of the open boundary and outflow through the Norwegian trench along the eastern side [*Lee*, 1980]. The large majority of this North Atlantic input is steered along the topographic boundary separating the northern and southern regions, and therefore, only a small fraction reaches the shallow southern North Sea. A smaller input of North Atlantic water enters the southern regions via the English Channel.

The main freshwater sources are the major rivers of the European continent, which discharge along the southern and southeastern coast of the North Sea and join the relatively fresh continental coastal water mass (CCW) [*Lee*, 1980]. The CCW flows northeasterly along the coast and is also fed by an outflow from the Wadden Sea, which extends for over 500 km along the Dutch, German, and Danish coasts (Figure 1). The Wadden Sea, spanning approximately 5000 km^2, consists of sandy and muddy tidal flats, most of which are exposed at low tide. Small rivers, controlled freshwater release from sluices ("siels" or small lockable waterways), as well as fresh and brackish submarine groundwater discharge all enter the Wadden Sea before being flushed through a series of tidal channels into the southeastern bight (SEB) region of the North Sea. The flushing time for these waters is estimated at about 4 days [*Moore et al.*, 2011]. Over a tidal cycle, organic material from the North Sea is imported into the Wadden Sea as the tide rises, with subsequent export of remineralized inorganic substances back into the North Sea during the falling tide. While the contribution of freshwater from the Wadden Sea is relatively minor, this tidal exchange of dissolved and particulate materials is an important process in the biogeochemistry of the North Sea [*Thomas et al.*, 2009; *Moore et al.*, 2011]. Low-salinity Baltic Sea water also enters the North Sea from the east via the Skagerrak (Figure 1).

The majority of North Sea sediments are permeable sands, with finer-grained and muddy sediments limited to small patches and to deeper regions of the Skagerrak and Norwegian trench [*Weisner et al.*, 1990; *Slomp et al.*, 1997]. In most regions, resuspension and remineralization during fall and winter months results in negligible annual sediment accumulation. Accumulation can occur near river mouths in the German Bight in the postglacial Elbe river valley and in the Norwegian trench area. These regions are also characterized by higher organic carbon content compared to the rest of the North Sea [*Weisner et al.*, 1990; *Slomp et al.*, 1997].

3. Methods

3.1. Sample Collection and Analysis

All data were obtained during a 3 week cruise in September 2011, aboard the R/V *Pelagia*. The cruise followed an approximate 1° × 1° sampling grid of the entire North Sea covering 88 total stations (Figure 1; for further details of typical North Sea sampling procedure, see *Bozec et al.* [2006]). Conductivity, temperature, and pressure profiles with accompanying rosette water sampling were done at every station. At 19 of these stations additional samples were collected using multiple deployments of zooplankton nets and a box corer.

Ra isotopes were collected from surface waters (at 5 m depth) at 61 stations. At 13 of these stations, two to three additional samples were taken near the sediment surface in 3–5 m vertical intervals in an attempt to capture chemical gradients near the sediment surface. In total, 99 water column samples were collected with sample volumes ranging from 80 to 212 L. Pore waters were sampled from box cores at seven stations using a type of pushpoint sampler (small metal tube with thin slits near the bottom) connected to a glass cylinder and extracted using a small vacuum pump. The pushpoint sampler was inserted approximately 30 cm into the core; thus, the measured values are considered average activities over approximately this depth. Sample volumes for pore water ranged from 0.7 to 1.1 L.

Further Ra sampling was done at 11 stations in conjunction with the sediment incubation team on board. Between 10 and 15 cm of undisturbed sediment collected using the box corer was subsampled into a benthic flux chamber and a further 10–15 cm of bottom water collected from the rosette was placed atop the sediment. To test the effect of water column turbulence on benthic fluxes, the overlying water was stirred at two different rates (40 and 80 revolutions per minute, RPM) using spinning plates suspended 10–15 cm above the sediment surface. Previous studies have shown the importance of the chamber geometry on the benthic boundary layer and therefore on solute fluxes through the sediment-water interface [*Santschi et al*., 1991; *Tengberg et al*., 2005]. Due to the short time on-station and the unknown sediment composition, it was not possible to adapt the chamber design or stirring rates to in situ conditions. Thus, two stirring rates were chosen to mimic a range of interfacial pressure gradients and solute exchange conditions [*Huettel and Gust*, 1992; *Janssen et al*., 2005b]. For more details on incubation methods, refer to Brenner et al. (manuscript in preparation, 2014). Following the incubations, which ranged from 12 to 24 h, the overlying water was removed for Ra analysis. Incubation sample volumes ranged from 3 to 8 L. A table of all samples collected is provided in Appendix A.

Water column samples were prefiltered through 10 μm and 1 μm filter cartridges placed in sequence and smaller volume incubation samples were passed through the 1 μm filter only. After prefiltering, all samples were pumped slowly (<1 L min^{-1}) through a MnO_2-coated acrylic fiber to extract Ra. Pore water samples were prefiltered by gravity before Ra extraction to conserve the smaller volumes. All samples were counted on board using the RaDeCC (Radium Delayed Coincidence Counting) system [*Moore and Arnold*, 1996]. For all samples, initial counts were made within 2 days of collection. A second count was made while on board, 7–13 days after initial collection, to determine the amount of supported ^{224}Ra present from the parent ^{228}Th isotope. At this time, between 9 and 38% of the initial ^{224}Ra remains on the fiber, which is corrected for using the activities obtained from both counts. A subset of 21 samples was counted a third time after about 5 months to determine an approximate value of the actinium parent of ^{223}Ra. The values of ^{224}Ra and ^{223}Ra listed here are therefore excess Ra activities.

Uncertainties for measurements of short-lived Ra isotopes are calculated using propagation of errors in various terms, including counting efficiency, volume estimates, as well as background and spurious counts. The initial source of error is defined by the standard 1σ counting statistics, where the fractional uncertainty for a particular Ra sample is proportional to the square root of the number of counts registered (i.e., if samples are counted for similar times, "hotter" samples will produce lower relative uncertainties). ^{224}Ra consistently exhibited count rates approximately 10X higher than those of ^{223}Ra, resulting in an average ^{224}Ra uncertainty (13%) approximately 3X lower than that of ^{223}Ra (36%).

Porosity data were obtained using an extensive data compilation done at the Helmholtz Zentrum Geesthacht. Data were compiled from a number of studies to create a fine-scale map of porosities throughout the entire North Sea (W. Puls, personal communication, 2013). A coarser-scale grid ($0.25° \times 0.25°$) was then made by binning data from the fine-scale map. Using the precise coordinates of the relevant stations (see Appendix A), porosities were then assigned directly from this grid. Thus, each value represents an average of between 16 and 36 porosity measurements made within that grid cell. Mean grain size distribution was determined during the cruise using a Malvern Mastersizer 2000 particle analyzer.

Mixed layer depths were determined using profiles of potential density anomalies (σ_θ) and are defined as the depth where the change in σ_θ from the surface bottle exceeds 0.1 kg m^{-3}. Potential density anomalies are calculated based on temperature, salinity, and pressure of a given water sample, and using a reference surface pressure of 0 dbar.

3.2. Flux Calculations From Incubations

Benthic fluxes of Ra are calculated according to methods proposed by *Hancock et al*. [2000] for fluxes in benthic chambers. Assuming the flux out of sediments F (dpm m^{-2} d^{-1}) is constant, the change in Ra activity (dpm: atoms decaying per minute) in the overlying water A_{olw} (dpm m^{-3}) during the incubation time t (days) can be described as

$$\frac{dA_{olw}}{dt} = \frac{F}{A} - \lambda A_{olw}, \tag{1}$$

where λ is the decay constant for the respective Ra isotope and H is the height of the overlying water assuming a well-mixed water column. Assuming the activity at the beginning of the incubation ($A_{t=0}$) is equal to the near-bottom water column activity, which was measured (see above), the above equation can be solved and rearranged as follows:

$$F = \frac{H\lambda}{1 - \exp(-\lambda t)}[A_{olw} - A_{t=0}\exp(-\lambda t)]. \tag{2}$$

Uncertainties in the benthic flux are calculated by applying the uncertainty propagation for uncorrelated variables formula to equation (2).

3.3. Radium Inventories

Ra inventories are calculated based on the assumption that a single surface measurement represents the activity throughout the mixed water column. This assumption is reasonable given that seven out of eight vertical profiles measured in the SNS show constant activities with depth (station 11 shows slight enrichment near the bottom). The Ra inventory, then, is the surface Ra activity (in dpm m^{-3}) multiplied by water depth. In the stratified NNS, surface inventories are calculated using the depth of the surface mixed layer. Uncertainty for a given Ra inventory is calculated using the uncertainty in the corresponding Ra activity.

At steady state, the Ra inventory of a m^2 water column with a lone benthic Ra source and no exchange with surrounding waters is a function of the benthic flux and the decay constant. Thus, if an assumption is made that no other Ra sources or sinks exist at a particular location, the inventory can be used to back calculate a water column-based estimate of the average benthic Ra flux.

3.4. Ra Mass Balance

Building a Ra mass balance and solving for the sedimentary input provides a third independent approach to estimating the benthic flux. The distribution of Ra represents a balance of Ra sources and sinks from a variety of locations throughout the North Sea. If we consider the SEB of the North Sea and assume that the sources of Ra to the region are balanced by the sinks (i.e., steady state), a surface water Ra mass balance, rearranged to solve for sedimentary input, can be written as follows:

$$Q_{Sed} = Q_{Decay} + Q_{Mix} - Q_{WS} - Q_{Riv} - Q_{SPM}, \tag{3a}$$

$$F_{Sed} = \frac{Q_{Sed}}{A_{SEB}}, \tag{3b}$$

where inputs are the efflux from SEB sediments (Q_{Sed}), the addition from the Wadden Sea (Q_{WS}), the river flux (Q_{Riv}), and a potential source from suspended particulate matter (SPM) in the SEB (Q_{SPM}). To balance these inputs, Ra is lost by decay (Q_{Decay}) and via exchange with lower activity waters outside the SEB (Q_{Mix}). A simple schematic describing the mass balance setup is shown in Figure 2. Units for sources and sinks are dpm d^{-1}; thus, dividing Q_{Sed} by the surface area of the SEB (A_{SEB}) provides a flux term (F_{Sed}) in the appropriate units.

The input of Ra from the Wadden Sea is calculated using a similar approach as *Moore et al*. [2011], who computed Ra loss from the Wadden Sea to the open North Sea using an equation of the form

$$Q_{WS} = \{[V_{WS}(Ra_{WS} - Ra_{SEB})]/\tau_{WS}\}. \tag{4}$$

Ra_{WS} and Ra_{SEB} are the average Ra activities of the Wadden Sea and SEB, respectively, τ_{WS} is the approximate time scale of mixing between Wadden Sea tidal flats and the SEB, and V_{WS} is the estimated volume of the Wadden Sea. Equation (4) is also used to estimate the loss of Ra from the SEB via mixing with the rest of the North Sea (Q_{Mix}), using corresponding mixing time scales (τ_{SEB}) and average Ra activities for all North Sea samples taken outside the SEB (Ra_{NS}). Q_{Decay} is the product of the SEB volume (V_{SEB}), Ra_{SEB}, and the

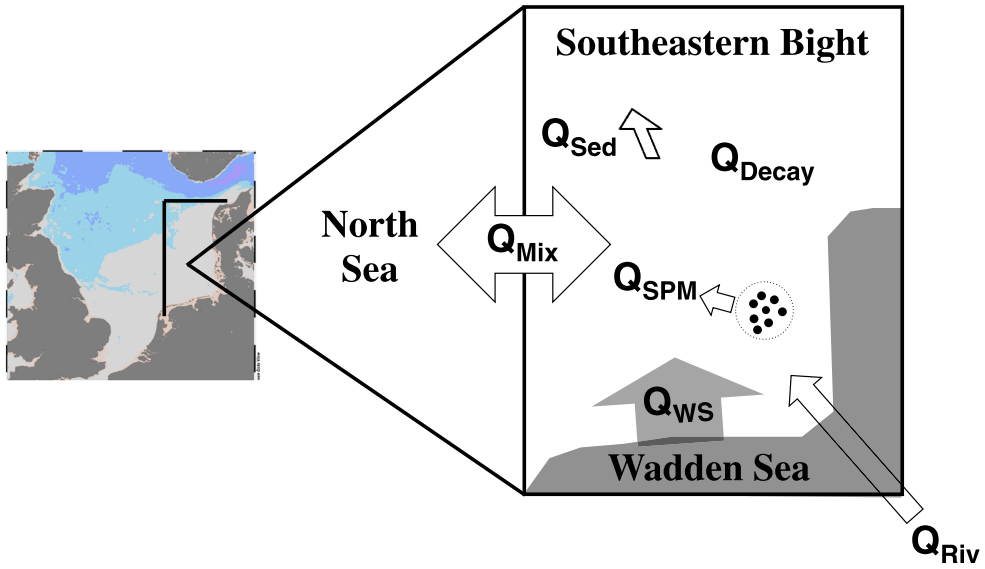

Figure 2. Schematic showing the location of the Southeastern Bight (SEB) and the mass balance setup. Q_{Riv} is the sum of four river inputs. Q_{SPM} is the Ra given off from suspended particles in the water column, shown as small black circles. Q_{Sed} is shown as an arrow coming out of the seafloor.

decay constant (λ). Q_{Riv} is approximated using the total freshwater discharge into the SEB multiplied by the riverine Ra activity (Ra_{Riv}). Finally, Q_{SPM} is the product of the previously reported sediment desorption rate of Ra, an approximation for SPM in the SEB, V_{SEB}, and λ. All terms used in the mass balance, as well as the source for these values, are listed in Table 1.

Table 1. Values Used in Mass Balance Model

Variable	Value		Source
SEB surface area (m^2) [a]	1.4×10^{11}		*Thomas et al.* [2009]
SEB volume (m^3)	4.5×10^{12}		*Thomas et al.* [2009]
WS surface area (m^2)	5.0×10^{9}		*Thomas et al.* [2009]
WS average depth (m)	5		This work
Flushing of SEB, τ_{SEB} (d)	42		*Thomas et al.* [2009]
Flushing of WS, τ_{WS} (d)	4		*Moore et al.* [2011]
SPM (mg L^{-1}) [b]	2		*Holt and James* [1999]
SEB river discharge (m^3 d^{-1}) [c]	1.5×10^{8}		*Pätsch and Lenhart* [2011]
	^{224}Ra	^{223}Ra	
Ra_{WS} (dpm 100 L^{-1})	46.0	2.4	*Moore et al.* [2011]
Ra_{SEB} (dpm 100 L^{-1})	5.7 ± 0.5	0.8 ± 0.2	This work
Ra_{NS} (dpm 100 L^{-1})	3.9 ± 0.4	0.5 ± 0.1	This work
Ra_{Riv} (dpm 100 L^{-1}) [d]	20.0	1.1	*Moore et al.* [2011] and others
Lambda (d^{-1})	0.19	0.06	
Desorption rate (dpm g^{-1}) [e]	2	0.1	*Moore et al.* [2011]
Q_{decay} (dpm d^{-1})	4.9×10^{13}		
Q_{Mix} (dpm d^{-1})	1.9×10^{12}		
Q_{WS} (dpm d^{-1})	2.5×10^{12}		
Q_{Riv} (dpm d^{-1})	2.8×10^{10}		
Q_{SPM} (dpm d^{-1})	3.4×10^{12}		
Q_{Sed} (dpm d^{-1})	4.5×10^{13}		

[a] Lowered slightly from *Thomas et al.* [2009] to account for the fact that sediments within the small, stratified area of the SEB will not contribute to Q_{Sed}.
[b] Average of September observations from a SNS cruise.
[c] Combined annual average discharges of Elbe, Weser, and Ems Rivers, as well as Lake Ijessel.
[d] Maximum activity measured by *Moore et al.* [2011] in a small channel emptying into the Wadden Sea. Similar activities have been measured elsewhere [*Moore et al.*, 2006; *Kelly and Moran*, 2002].
[e] Equal to activity of parent isotope, assuming 100% desorption. ^{227}Ac on sediments estimated to be 5% of ^{228}Th.

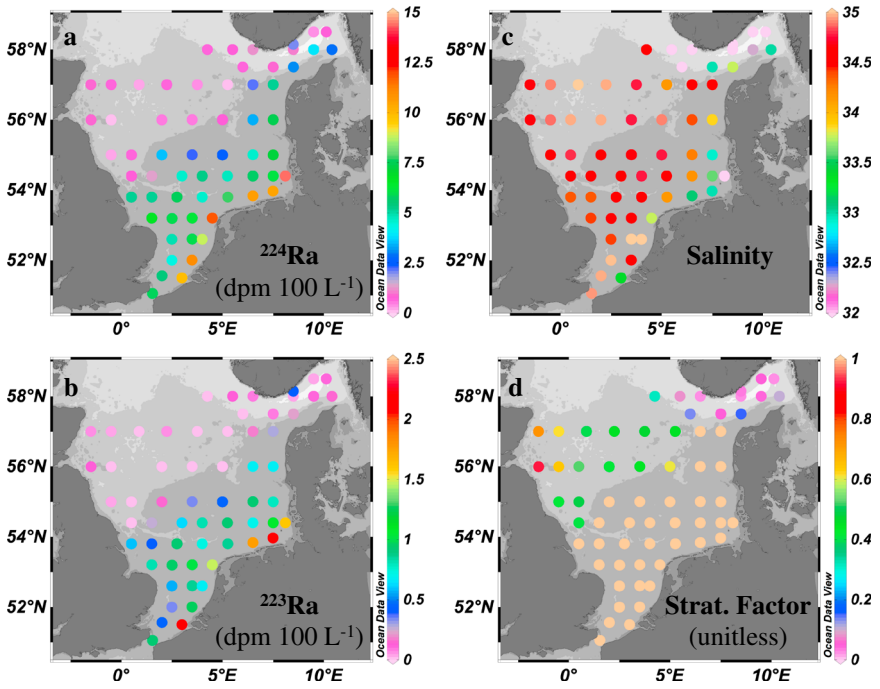

Figure 3. Surface distributions of (a) ^{224}Ra, (b) ^{223}Ra, (c) salinity, and (d) stratification factor in the North Sea. Stratification factor (SF) is the mixed layer depth divided by water column depth, so a SF of 1 indicates a fully mixed water column. Note the different color scales between the two Ra distributions. The depth contours shown are the same as in Figure 1.

3.5. Passive Tracer Modeling

Surface Ra distributions in the North Sea are reproduced using Ra as a decaying passive tracer in the 3-D hydrodynamic module of the coupled physical-biological ECOSMO model (ECOSystem MOdel) [*Schrum et al.*, 2006; *Daewel and Schrum*, 2013], which has earlier been extensively validated. The model uses a 20 min time step, with 6′ × 10′ horizontal resolution, a vertical grid of 5 m in the upper 40 m, and a decreasing vertical grid resolution below that depth. The current model version has been equipped by a less diffusive and more accurate total variation diminishing scheme which ensures preservation of realistic spatial structures which is shown by rigid validation against FerryBox observations [*Barthel et al.*, 2012]. In separate runs, Ra was added from three distinct sources: the sediments, using the average of the inventory and mass balance fluxes (see section 4 and Table 3 below), the Wadden Sea, using the rate calculated in the mass balance (Q_{WS}), and from rivers, using an estimate for riverine Ra (Table 1) and the average monthly discharges already present in the model. Both sedimentary and Wadden Sea inputs are held constant throughout the model runs, the implications of which are discussed in section 4.5.

For each model run, we can quantify and illustrate the quality of the fit between simulated activities and our observations using a method described by *Taylor* [2001]. For a given simulation, the numerical difference between modeled activities and observed activities is quantified as the root-mean-square (RMS). The pattern similarity between the observational and model data is measured by calculating the correlation coefficient (CC). Finally, the standard deviation (SD) in the modeled data set is compared to that of the observations. All three parameters (RMS, CC, and SD) are plotted on a single Taylor diagram, thus providing a comprehensive illustration of how well each model run describes the observations.

4. Results and Discussion

4.1. North Sea Ra Distributions and Sources

The surface distributions of the two short-lived Ra isotopes show similar patterns (Figures 3a and 3b). The highest Ra activities, ranging from 7.6 to 14.6 dpm 100 L^{-1} for ^{224}Ra and 0.7 to 2.2 dpm 100 L^{-1} for ^{223}Ra, are consistently observed at the lower salinity stations near to the Belgian, Dutch, German, and Danish coastlines, in the continental coastal waters (CCW). Although activities decrease further offshore, they remain

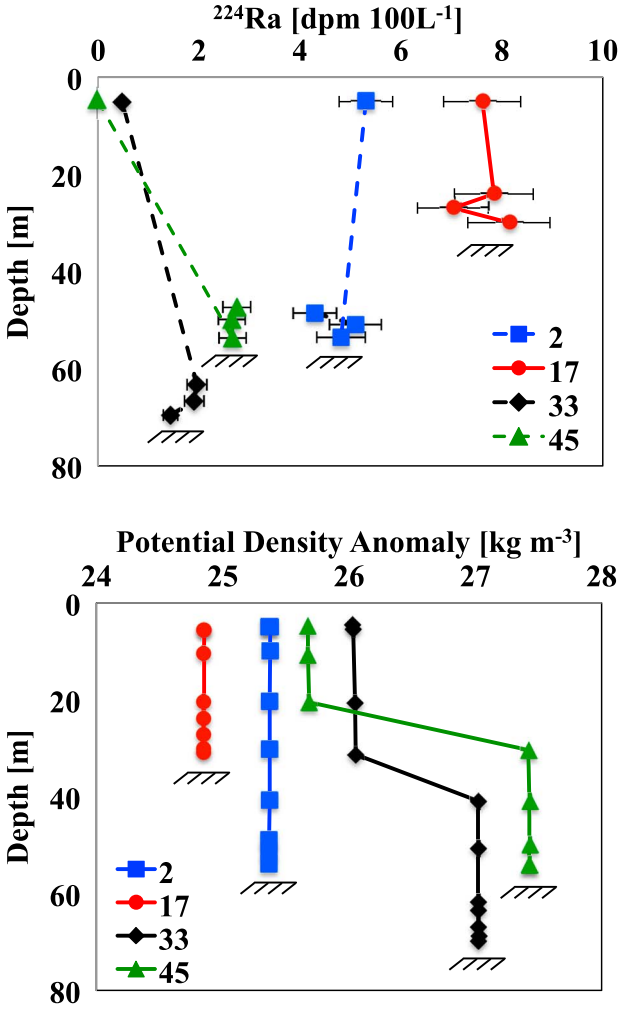

Figure 4. Vertical profiles of (top) ^{224}Ra and (bottom) density. Dashed lines are used in profiles where larger sampling gaps exist in the intermediate water column. Feathers beneath profiles indicate the depth of the sediment surface.

high throughout the entire SNS, from 2.2 to 7.5 dpm 100 L^{-1} for ^{224}Ra and 0.3 to 0.9 dpm 100 L^{-1} for ^{223}Ra. In the NNS, almost all ^{224}Ra activities drop to less than 1.0 dpm 100 L^{-1}, while ^{223}Ra is near to or, in many cases, below the detection limit. Though difficult to distinguish on the large-scale map, stations 66 and 67, at the mouths of the Norwegian Otra and Sira Rivers, respectively, have slightly elevated Ra (1.9 and 1.1 dpm 100 L^{-1} for ^{224}Ra, 0.4 and 0.1 dpm 100 L^{-1} for ^{223}Ra) compared to other NNS stations.

Vertical distributions of Ra mimic the patterns in potential density anomalies (Figure 4). In the SNS (Figure 4, stations 2 and 17), the constant density profiles confirm a well-mixed water column, and Ra activities are constant within the error margins. For stations in the NNS (Figure 4, stations 33 and 45), activities near the bottom are consistently higher than at the surface, where they drop toward the detection limit. These near-bottom enrichments, however, are relatively small compared to the high activities observed throughout the entire water column in all SNS stations.

The water column distributions of Ra, salinity and the stratification factor (Figures 3 and 4) clearly indicate two Ra sources for the North Sea. First, the combination of runoff from European continental rivers and discharge from the Wadden Sea make up a coastal source, which is likely to support the highest Ra activities observed in the CCW. This is reasonable given that rivers are a well-known source of Ra, and significant Ra release from the Wadden Sea tidal channels has been observed in previous studies [*Schmidt et al.*, 2010; *Moore et al.*, 2011]. Second, consistently high Ra activities throughout the SNS point to a sedimentary Ra source. Sediments are a well-documented source of short-lived Ra [*Hancock et al.*, 2006; *Moore*, 2007; *Colbert and Hammond*, 2008; *Burt et al.*, 2013a] and strong vertical mixing in shallow regions of continental shelves has been shown to cause localized surface enrichments in ^{224}Ra too far offshore to be caused by lateral transports originating from the coast [*Burt et al.*, 2013b]. While previous Ra studies in the region report undetectable short-lived Ra beyond 60 km offshore of the Wadden Sea [*Schmidt et al.*, 2010; *Moore et al.*, 2011], the substantially greater sample volumes collected here (1.5–3X larger than previous work) allow for a better detection limit of low Ra signals.

In contrast to the CCW, no significant short-lived Ra source is observed from the British or Norwegian coastlines. Slightly higher activities are observed along the northern British coast, but this may be related to the large increase in mixed layer depth (Figure 3d) bringing surface waters closer to the sediment source. Minor Ra enrichments near the Norwegian coast are likely due to localized river sources. The lack of a substantial Ra source from either Norwegian and British coasts is likely due to a combination of smaller river discharges in general, and to differences in surficial and bedrock geology in these regions compared to the European continental coast.

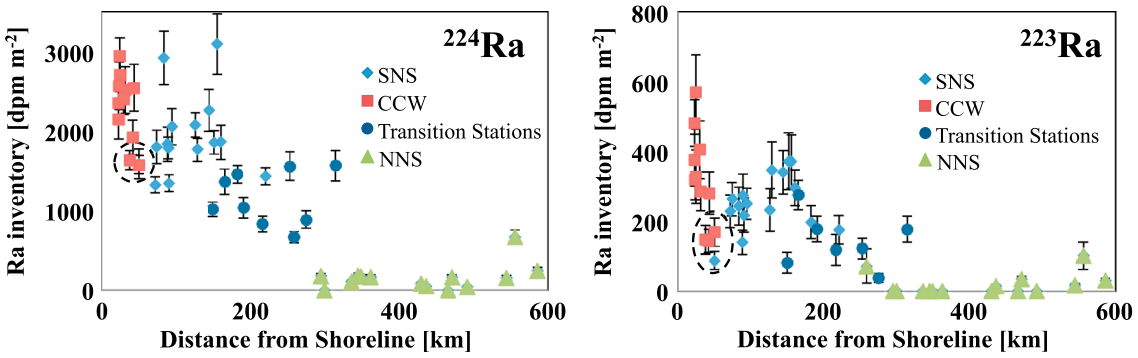

Figure 5. Ra inventories ((left) ^{224}Ra and (right) ^{223}Ra) plotted in transect away from the European continental coast. SNS stations (blue diamonds) are averaged to obtain the estimate of sedimentary Ra flux. Transition stations (blue circles) refer to stations bordering the NNS and SNS and indicate mixing between these two regions. Black dashed circles show low values along the Danish coast.

Baltic Sea waters entering via the Skagerrak do not appear to be a discernable source of short-lived Ra to the North Sea despite its coastal origin and correspondingly low salinities. While activities may indeed be higher in the Baltic Sea, the short half-lives of these isotopes likely prevent significant transport into the Skagerrak. Also, Baltic Sea water entering the Skagerrak flows over a steep drop in topography, isolating surface waters from benthic Ra inputs. It remains unclear from the limited number of data points whether North Atlantic waters entering via the English Channel supply a small additional input of short-lived Ra to the SNS.

Water depths in the North Sea increase with distance away from the continental coast. Therefore, in the fully mixed SNS, surface activities will be diluted as the depth of the water column increases if sedimentary sources dominate. This suggests the use of vertical Ra inventories (dpm m^{-2}) to further investigate the sources of short-lived Ra to the North Sea. Mixed layer Ra inventories of both short-lived isotopes are plotted with distance from the continental coast (Figure 5). Similar to the activity distributions, Ra inventories are highest in the CCW, with the largest Ra inventories found at stations near the mouths of the Rhine, Weser and Elbe, and Scheldt Rivers. However, low Ra inventories within the CCW are found at stations bordering the Danish coastline (see Figure 5). This indicates a lack of a coastal Ra source at this region of coastline that is not as apparent using activity distributions alone.

Stations in the SNS, characterized by a fully mixed water column (stratification factor =1, Figure 3d) show consistently high Ra activities and inventories. In fact, beyond the CCW, at regions from 70 to 160 km offshore, Ra inventories remain constant or even increase with distance away from shore. These findings indicate that the high activities are maintained by benthic input. Therefore, we conclude that bottom sediments, rather than the continental coastline, are the dominant source of Ra to the North Sea.

Once released from sediments, Ra will be immediately mixed into surface waters of the SNS, whereas in the deeper stratified stations of the NNS the benthic source is not in direct contact with surface waters. The lack of any local source results in near-background activities in NNS surface waters, as well as very low mixed layer inventories ($<$400 dpm m^{-2} for ^{224}Ra and $<$100 dpm m^{-2} for ^{223}Ra). Below the mixed layer, near-bottom activities are slightly higher because of the benthic source (Figure 4). Intermediate mixed layer inventories (500–1100 dpm m^{-2}) at stations between 200 and 330 km offshore (i.e., bordering the SNS and NNS) imply mixing of stratified NNS waters with the shallow, sediment-supported SNS waters.

4.2. Independent Estimates of Benthic Ra Flux

The bottom sediments have been identified as the dominant source of short-lived Ra to the North Sea. Therefore, the following section details the quantification of this benthic source using three independent approaches: sediment incubations, mixed layer inventories, and mass balance.

4.2.1. Incubation-Based Ra Fluxes

Pore water activities were in excess of a hundred times higher than the majority of water column samples, ranging from 6.5 to 10.9 dpm L^{-1} for ^{224}Ra and 0.4 to 1.1 dpm L^{-1} for ^{223}Ra (Table 2). A benthic Ra flux is generated when these high Ra pore water activities are transported across the sediment-water column interface. We have carried out incubation experiments in order to directly quantify sediment-water column exchange of Ra. Significant Ra enrichments were observed in the overlying water column following all

Table 2. Results From ^{224}Ra Sediment Incubations and Pore Water Sampling, Including Comparison to Literature Values

Station	Sediment Description[a]	Ra Flux 40 RPM (dpm m^{-2} d^{-1})	Ra Flux 80 RPM (dpm m^{-2} d^{-1})	Pore Water (dpm L^{-1})	Water Flux[b] (L m^{-2} d^{-1})
7	medium sand	48.0 ± 9.1	220.5 ± 27.3	-	5.7 ± 1.2[c]
2	medium sand	70.6 ± 9.5	153.5 ± 18.0	-	8.4 ± 1.4[c]
11	medium sand	35.4 ± 8.9	58.4 ± 8.7	6.4 ± 0.7	5.5 ± 1.5
17	fine sand	108.2 ± 17.1	-	8.7 ± 1.0	12.4 ± 2.4
20	fine sand	139.7 ± 82.4	-		16.7 ± 3.1[c]
32	fine sand	88.4 ± 11.2	256.3 ± 29.7	7.3 ± 0.9	12.1 ± 2.1
30	fine sand	242.8 ± 32.7	218.6 ± 37.1	9.4 ± 1.1	25.7 ± 4.5
38	fine sand	164.4 ± 19.5	195.0 ± 22.3	10.9 ± 0.8	15.1 ± 2.1
45	medium sand	50.6 ± 7.8	122.3 ± 13.4	10.5 ± 0.7	4.8 ± 0.8
62	coarse silt	282.0 ± 18.8	-	-	33.7 ± 4.1[c]
65	coarse silt	60.3 ± 7.5	-	-	7.2 ± 1.2[c]
42	fine sand	-	-	5.4 ± 0.4	-
Average[d]		117.3 ± 82.4	174.9 ± 68.1	8.4 ± 2.1	13.4 ± 9.1
Study	Sediment Description	Reported Ra Flux (dpm m^{-2} d^{-1})		Pore water (dpm L^{-1})	Water Flux (L m^{-2} d^{-1})
Moore et al. [2011]	Wadden Sea Muds	97		9.8 ± 2.3	17.0
Colbert and Hammond [2008]	Beach Sands	368		8.2 ± 4.2	27.0
Moore et al. [2006]	Salt Marsh	175		5.0	33–36
Hancock et al. [2006]	Great Barrier Reef	202		-	-
Hancock et al. [2000]	Silts-Clays	228		12–36	-

[a]Wentworth scale definitions based on measurements of mean grain size.
[b]Ra flux at 40 RPM divided by pore water activity.
[c]Calculated using average pore water activity.
[d]Standard deviation of all samples (i.e., measure of the spatial variability).

sediment incubations, with calculated benthic fluxes ranging from 35 to 282 dpm m^{-2} d^{-1} for ^{224}Ra and 0.7 to 11.1 dpm m^{-2} d^{-1} for ^{223}Ra. For stations where incubations were conducted at both stir rates (i.e., turbulence regimes), observed ^{224}Ra fluxes at 80 RPM were higher than those at 40 RPM, with the exception of station 30, where the 2 values fall well within each other's error margins (Table 2).

Uncertainties in pore water ^{224}Ra activities range from 8 to 12%. Benthic flux uncertainties ranged from 7 to 25% for ^{224}Ra and scale with the relative uncertainties of the ^{224}Ra activities before and after incubations (see Table 2). Due to the low volumes sampled, the total number of ^{223}Ra counts registered for incubation and pore water samples ranged from 6 to 37 and 22 to 60 counts, respectively. Such low count rates result in >50% uncertainties for the majority of individual samples, creating uncertainties in the fluxes that range from 21 to 205%. Results from ^{223}Ra incubations are not reported in Table 2, but the overall average fluxes are shown later in Table 3 for comparative purposes.

4.2.2. Inventory-Based Benthic Flux

In order to calculate benthic Ra fluxes from inventories, stations with an assumed sole benthic source must be isolated. To do this, we ignore stations in the CCW, which are affected by coastal inputs, and transition stations, which lose Ra to the adjacent NNS, as well as NNS stations themselves, where surface waters are isolated by stratification (see Figure 5). Using the remaining stations, we obtain average ^{224}Ra and ^{223}Ra inventories of 1889 ± 185 dpm m^{-2} and 252 ± 54 dpm m^{-2}, respectively, which correspond to benthic Ra fluxes of 358 ± 35 dpm m^{-2} d^{-1} for ^{224}Ra, and 15.8 ± 3.3 dpm m^{-2} d^{-1} for ^{223}Ra. These fluxes, which are

Table 3. Comparison of Ra Benthic Flux Estimates

Method	Spatial Scale Considered	^{224}Ra (dpm m^{-2} d^{-1})	^{223}Ra (dpm m^{-2} d^{-1})
Incubations[a]	Entire sample area	146 ± 18	6.4 ± 3.4
Inventories	Subset of SNS	358 ± 35	15.8 ± 3.3
Mass balance	SEB (see Figure 2)	333 ± 40	17.7 ± 5.8

[a]Average (mean) and standard deviation of the 40 RPM and 80 RPM results from Table 2.

based on in situ water column observations, are consistently higher than those calculated using laboratory core incubations (2.5X for both isotopes; see Table 3). Further comparisons between the calculated fluxes are discussed in detail in section 4.3.

Inventories in the SNS show substantial variability. This variability is likely due to changes in water depth over small spatial scales, high tidal currents, and horizontal advection of waters over regions of variable topography. For example, station 15 (~160 km offshore), with the largest observed inventory for both isotopes, is located in a narrow canyon feature with shallower water depths to the immediate north and south. As discussed later, spatial variations in sediment characteristics affect the Ra flux, which will create some variability in the average inventory calculation.

4.2.3. Ra Mass Balance

For the ^{224}Ra isotope, entering all calculated values from Table 1 into equations (3a) and (3b) and considering the uncertainties in the observed Ra activities both inside the SEB (Ra_{SEB}) and outside (Ra_{NS}) yields

$$F_{Sed} = \frac{4.90\times10^{13} + 1.94\times10^{12} - 2.52\times10^{12} - 2.79\times10^{10} - 3.42\times10^{12}}{1.35\times10^{11}} = 333 \pm 40 \ \text{dpm m}^{-2}\,\text{d}^{-1}.$$

Evident from this calculation are the relative contributions of each source and sink to the overall mass balance. For example, according to this result, Ra distribution in the SEB is essentially a balance between sediment flux, which accounts for 88% of the total inputs, and decay, which accounts for 96% of the losses. This is likely due to the combined effects of a large spatial scale and the short half-life of ^{224}Ra. Coastal sources are almost negligible because the signal does extend far enough offshore, and mixing becomes unimportant because it occurs over time scales (6 weeks, Table 1) that are much longer than the time scales of ^{224}Ra decay (~10 days). This finding is supported by the passive tracer model results (see section 4.5). The effect of spatial scale is tested by considering only the seven southernmost data points in the SEB and thereby reducing the SEB surface area by approximately 85%. After adjusting the Ra_{SEB} and Ra_{NS} appropriately, and reducing τ_{SEB} by half, the sediments and decay still provide 70% and 88% of the respective inputs and outputs, and we obtain a comparable F_{Sed} of 360 dpm m^{-2} d^{-1}. It is important to note also that according to the mass balance, suspended sediments are a stronger short-lived Ra source to the SEB than the Wadden Sea and major rivers combined. Future studies in turbid coastal waters like the SNS should be aware of this potentially important Ra source.

The reported uncertainty is equivalent to the maximum sensitivity of the calculation to uncertainties in the Ra_{SEB} and Ra_{NS} terms shown in Table 1. However, the uncertainty reported here should be considered a minimum estimate, as further unknowns exist in other input variables. Input from rivers, SPM and the Wadden Sea may be slightly overestimated as the higher end of available variables were chosen. Furthermore, terms such as Ra_{Riv} are uncertain, as these observations are not available for the region. However, the input terms Q_{Riv}, Q_{SPM}, and Q_{WS} are 1–2 orders of magnitude smaller than other terms in the mass balance (Table 1), so overestimations and uncertainties in these terms will have a negligible effect of the results.

4.3. Sediment-Water Ra Exchange: Important Mechanisms and Dominant Controls

As is shown in the previous sections, the short-lived Ra tracer can be utilized in a number of ways to quantify sediment-water column exchange in coastal systems. By further investigating sources of variability within the incubation-based values, conclusions are drawn regarding the dominant processes controlling benthic Ra fluxes, and in turn, the observed North Sea Ra distributions. Then, comparing flux results first between our three independent methods, and then between our results and prior studies reaffirms the importance of these processes.

4.3.1. Variability in Flux Incubations

Incubation-based fluxes vary substantially in the North Sea (see Table 2): some of this spatial variability can be explained by examining differences in sediment characteristics. Higher Ra fluxes are measured in cores with a smaller mean grain size (Figure 6a). Smaller grain sizes with a greater surface area to volume ratio generally contain more adsorbed Th, and therefore release more Ra per unit volume [*Cai et al.*, 2014]. The relationship between sediment porosity and ^{224}Ra efflux (Figure 6b) implies that given constant near-bottom stresses above sandy sediments, more Ra is released at higher porosities (i.e., smaller grain size).

The turbulence regime in the overlying water column also plays an important and concurrent role in determining the Ra flux. In permeable sandy sediments, which cover the majority of the North Sea, advection

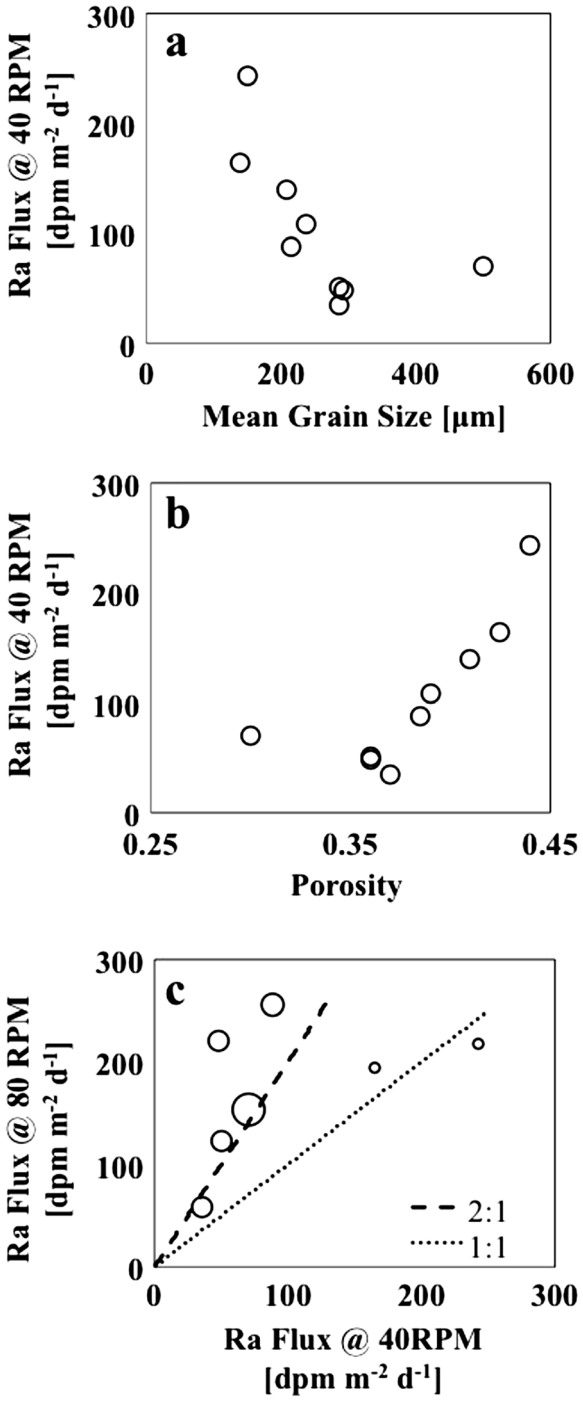

Figure 6. (a) Relationship between ^{224}Ra efflux and mean grain size. (b) Relationship between ^{224}Ra efflux and sediment porosity. (c) Effect of stirring rate on ^{224}Ra efflux. Size of symbols is directly proportional to the mean grain size in the sediment core (i.e., large circles represent coarser-grained sands).

via sediment irrigation is often considered the dominant physical process governing pore water transport [*Jahnke et al*., 2005]. The North Sea is also characterized by intense mixing and strong near-bottom currents, which will induce large-pressure gradients on the sandy sediments. Maximum tidal currents are significantly stronger in the SNS than in the NNS; thus, increased sediment-water column exchange via sediment irrigation is expected in the SNS. In sediment incubations, where water column turbulence regimes can be held constant (i.e., at 40 RPM) no patterns between SNS and NNS stations are evident. Likewise, no regional pattern in sediment characteristics exists between these two regions.

For incubations, different sediments respond differently to an increase in stirring rates. In coarser sands, doubling the stirring rate results in a near doubling of the benthic Ra flux, while in finer-grained, more cohesive sediments, fluxes for both stirring rates fall close to a 1:1 line (Figure 6c). Sediment irrigation, which is the dominant transport mechanism in coarse (i.e., permeable) sands, will be increased at higher turbulence regimes, while water column turbulence has a lesser or negligible effect in finer grained (i.e., less or impermeable) sediments. Therefore, while maximum Ra fluxes are found at stations with smaller grain size with larger pore water volume (i.e., higher porosity), Ra efflux is eventually limited by decreases in permeability at very fine grain sizes.

Sediment characteristics do not appear to play a role in the deep waters of the Skagerrak, where our two stations, 62 (308 m depth) and 65 (534 m depth), which are very similar in terms of sediment types (high porosity, small mean grain size), have vastly different incubation ^{224}Ra fluxes (282 dpm m^{-2} d^{-1} and 60 dpm m^{-2} d^{-1}, respectively). In situ observations confirm this difference in ^{224}Ra efflux, with near-bottom ^{224}Ra activities ranging from 3.7 to 5.3 dpm 100 L^{-1} and 0.6 to 1.7 dpm 100 L^{-1} for the two respective stations. Different near-bottom turbulence regimes may exist on the shallower slope (Station 62) compared to the bottom of the Norwegian trench (Station 65), but the exact causes for this substantial difference in benthic Ra flux is not clear from our observations. Focused sampling across the steep Norwegian trench could be of interest for future study.

In summary, our results show that both the turbulence regime and the sediment characteristics exert the major controls on the observed Ra fluxes across the North Sea. However, while the shallower SNS experiences much more turbulent conditions than the deeper NNS, sediment characteristics in turn do not reveal clear spatial patterns across the North Sea. As a consequence, there does not appear to be a clear relationship between the magnitude of the Ra fluxes and the geographical location of the station only (i.e., between Ra fluxes and stratification conditions only).

4.3.2. Comparing Flux Results

The importance of the turbulence regime in the overlying water column is evident when comparing sedimentary ^{224}Ra and ^{223}Ra fluxes computed using all three approaches (Table 3). For both isotopes, considerably larger fluxes are calculated using methods based on in situ observations (inventory and mass balance) compared to those obtained using incubations. This suggests that the prescribed mixing conditions of the onboard laboratory incubations significantly underrepresent the conditions present in this region, resulting in underestimated rates of sediment-water column exchange. This is unsurprising given that the incubation experiments aim to recreate pore water exchange through irrigation without inducing sediment resuspension [*Janssen et al*., 2005b]. Given the high turbidity observed in the water column of the SNS, sediment resuspension was undoubtedly occurring in this region during the cruise. The inability to reconstruct physical conditions near the sediment-water interface is a well-documented limitation of incubation chambers in general [*Lohse et al*., 1996; *Jahnke et al*., 2000; *Cai et al*., 2012]. In the North Sea, prior discrepancies in pore water profiles between laboratory and field studies has been attributed to intense wave action and tidal currents [*Lohse et al*., 1996]. Despite this, incubation results show clear geographical and hydrodynamical variation in the fluxes, and thus provide valuable information regarding the dominant controls on benthic Ra fluxes in the North Sea.

Fluxes based on inventories and mass balance are high when compared to a variety of studies that calculated Ra fluxes in different coastal systems (Table 2). *Moore* [2007] compiled Ra flux estimates for fine-grained sediments, yielding rather consistent values around 225 dpm m^{-2} d^{-1}. The majority of these studies took place in estuarine settings (lagoons and marshes), where permeability is likely lower and physical conditions near the sediment surface are likely less turbulent compared to the conditions found in the SNS. In similarity to our results, *Colbert and Hammond* [2008] calculated higher Ra fluxes (368.2 dpm m^{-2} d^{-1} for ^{224}Ra and 21.9 dpm m^{-2} d^{-1} for ^{223}Ra) at the sandy shoreline of San Pedro Bay (USA), where breaking waves were thought to induce considerable sediment-water column exchange. *Cai et al*. [2014] observed very high ^{224}Ra fluxes in the Yangtze estuary, ranging from 170 to 1780 dpm m^{-2} d^{-1}, and concluded that sediment irrigation is responsible for 70% of the total benthic flux. Direct comparison between their Ra/Th disequilibrium method and separate incubation results revealed that in the shallow, turbulent estuarine region, incubation results greatly underestimated the flux, which is in agreement with our findings reported above, while in deeper outer shelf sediments, both methods yielded similar values (P. Cai, personal communication, 2013).

The activity of Ra in the pore waters of North Sea sediments appears comparable to the majority of previous studies (Table 2); thus, the higher Ra fluxes calculated by both inventory and mass balance methods likely reflect higher rates of sediment irrigation induced by the strong mixing conditions of the SNS. Further to these rather physical considerations, bioturbation also enhances sediment-water column exchange, and thus higher Ra fluxes, especially in the SNS where densities of benthic macrofauna are generally quite high [*Dauwe et al*., 1998].

It is clear from these results that sediments release a considerable amount of Ra enriched pore water into the water column. These same pore waters are likely enriched in other chemical species, such as nutrients, metals, and carbon species, suggesting that sediment-water column interaction plays an important role in other North Sea chemical budgets.

4.4. Pore Water Fluxes and Implications for Carbon Biogeochemistry

Pore water measurements taken from North Sea box cores compare well to values published in previous studies (Table 2). Compared to samples taken in the Wadden Sea by *Moore et al*. [2011], the values fall within the error margins of each other. Dividing the Ra efflux (dpm m^{-2} d^{-1}) by the pore water activity (dpm L^{-1}) yields estimates of the volume flux through sediments. For incubation samples, volume fluxes vary from 5.5 to 25.5 L m^{-2} d^{-1} for ^{224}Ra and 1.1 to 10.0 L m^{-2} d^{-1} for ^{223}Ra (Table 2). If we consider the inventory and

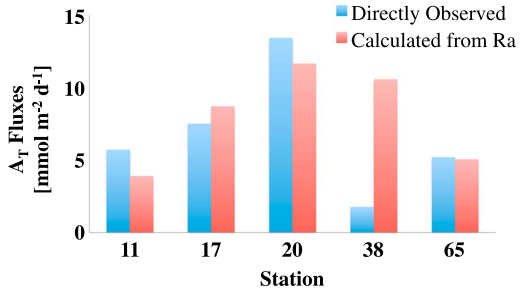

Figure 7. Comparison of Ra-based alkalinity fluxes to those calculated directly in sediment incubations. Incubation data from Heiko Brenner (manuscript in preparation, 2014).

mass balance approaches to better represent in situ sediment-water column exchange in the North Sea, then using the corresponding ^{224}Ra fluxes in Table 3 and the average pore water ^{224}Ra activity, we obtain volume fluxes of 40–42 L m^{-2} d^{-1} in the North Sea. These values represent the extent of sediment-water column exchange by all potential mechanisms and compare well to previous estimates of volume fluxes, which are based on a variety of methods including a numerical model of nonlocal exchange [*Colbert and Hammond*, 2008] and laboratory experiments of wave-driven advection [*Precht and Huettel*, 2003]. The volume fluxes should be considered as upper limits, as they are based on Ra effluxes that include diffusive transport across the sediment-water interface, which does not involve volume exchange. Volume fluxes can be combined with estimates of pore water concentrations of nutrient or carbon species to estimate fluxes of those substances into the North Sea.

Sediment-water column exchange plays a key role in both carbon and nutrient cycling in coastal regions. This is especially true in the shallow SNS, where large quantities of organic matter are transported to and regenerated within sediments relatively rapidly. More specifically, alkalinity fluxes from sediments have been shown to contribute significantly to the carbon budget [*Thomas et al*., 2009] and to variations in air-sea exchange of CO_2 in the North Sea [*Omar et al*., 2010]. Here our Ra-based measurements of volume flux during incubations can be used to make a first-order estimate of incubation alkalinity fluxes. Since literature estimates of pore water A_T are not available in the open North Sea, we consider deep profiles of alkalinity (A_T) in Wadden Sea sediments during a multiyear time series as an appropriate substitute. Values of pore water A_T at both 0.05 and 1 m depths were around 3 mmol L^{-1} and showed very little variability during the time series [*Moore et al*., 2011]. Similar pore water A_T (~2.6 mmol L^{-1}) was measured in a Wadden Sea tidal channel by *Hoppema* [1990].

Taking the average water column A_T observed in the SNS during the cruise (2.3 mmol L^{-1}), excess A_T in pore waters is approximately 0.7 mmol L^{-1}, which multiplied by our estimates of water fluxes during incubations (Table 2), yields A_T fluxes from incubations ranging from 3.4 to 23.6 mmol m^{-2} d^{-1}. These values compare well to directly observed A_T fluxes from the on board incubations (Figure 7; Brenner et al., manuscript in preparation, 2014). The discrepancy at the lone NNS station (Station 38) may result from applying a single pore water A_T value to all stations in the Ra-based method. While both Ra pore water activities and fluxes in the SNS and NNS stations are similar (Table 2), observed A_T fluxes are consistently much lower in the NNS (H. Brenner, personal communication, 2014), suggesting that pore water A_T in these sediments is also lower.

Using an independent closing term approach, *Thomas et al*. [2009] estimated benthic A_T fluxes with a similar order of magnitude (9.6 mmol m^{-2} d^{-1}) throughout the southeastern bight and Wadden Sea during autumn. Like the Ra fluxes, our incubation-based A_T fluxes are likely lower than the in situ fluxes, especially in the SNS. However, more representative fluxes could be obtained using the volume fluxes mentioned above from the water column-based methods, which are based on in situ turbulence conditions.

In absence of other data, we make the assumption that pore water A_T in North Sea sediments can be approximated using data from the adjacent Wadden Sea. Also, we must assume that no reoxidation occurs between 5 cm depth, where the pore water was sampled [*Moore et al*., 2011], and the sediment-water interface. It is important to note that these A_T calculations represent an order of magnitude first estimate, and the comparisons are made simply to recognize the potential application of Ra-based volume fluxes.

4.5. Passive Tracer Study

In order to further corroborate the observation-based Ra fluxes, i.e., the Ra sources to the North Sea, we simulate the distributions of ^{224}Ra as a passive tracer using the hydrodynamic module of the ECOSMO model [*Daewel and Schrum*, 2013]. The ^{224}Ra sources (Table 3) are held constant throughout the run, except for the minor ^{224}Ra input related to time varying runoff. This means that any differences in surface Ra distributions

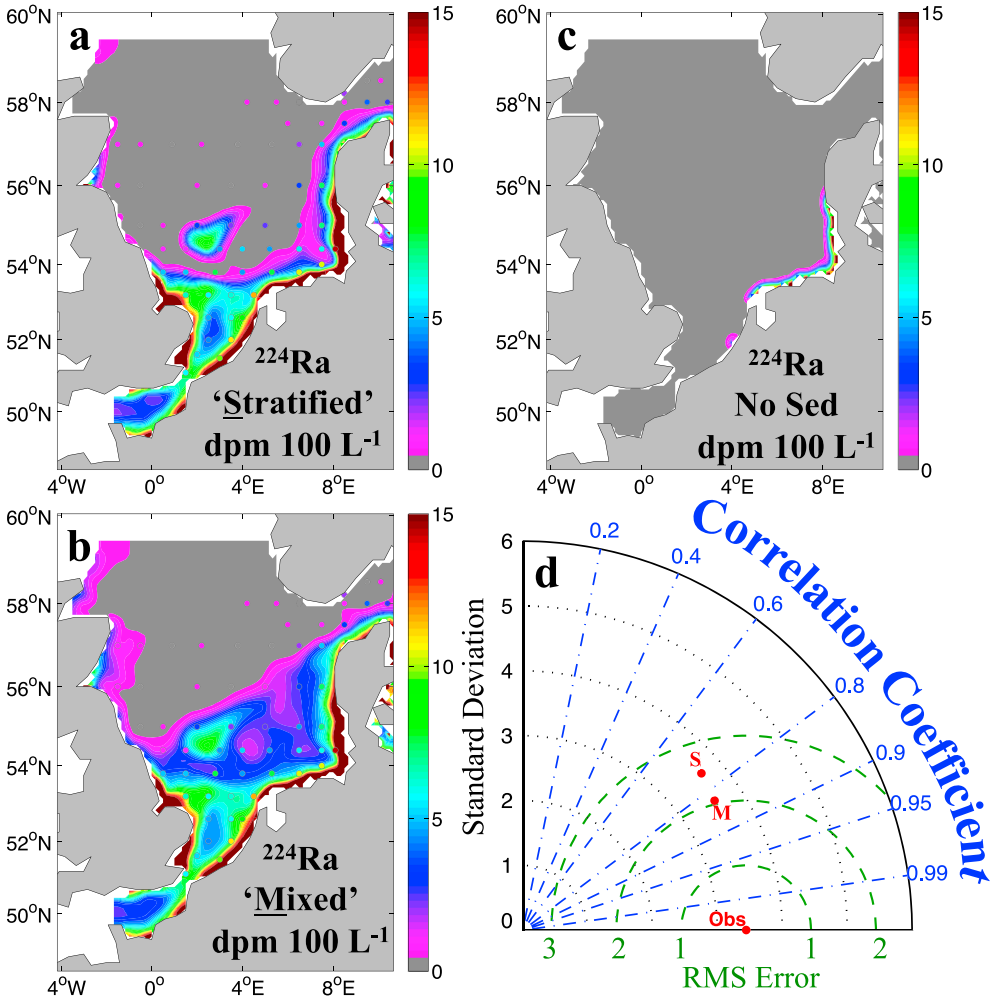

Figure 8. ECOSMO model output of mean ^{224}Ra distributions for (a) June to August 2007 (i.e., during seasonal stratification in the SNS) and (b) October to December 2007 (i.e., strong mixing in the SNS). Observations are overlain (small circles, same color scale) for comparative purposes. (c) ^{224}Ra distributions with sediment source removed. Here the annual average is shown because seasonality of this distribution is indistinguishable. (d) Taylor diagram for all ^{224}Ra observations and the simulation S (stratified water column, shown in Figure 8a) and M (mixed water column, shown in Figure 8b). Green curved lines are 1 dpm 100 L^{-1} contours of root-mean-square error between observations and model output; blue straight lines show correlation between observations and model output; and black dots represent the factor of standard deviation for each simulation compared to the standard deviation of the observations.

over time can be attributed entirely to changes in hydrographic conditions. Balancing the relatively short half-life of ^{224}Ra (3.7 days) with the time scales of turbulent mixing and molecular diffusion, the vertical structure of the water column—stratified versus vertically mixed—plays a crucial role in how the predominantly sedimentary ^{224}Ra inputs are reflected in the surface waters. The expectation is that in stratified waters transport of ^{224}Ra to surface waters is diffusion controlled. Thus, surface activities drop to undetectable levels because the time scale of diffusive transports is beyond the half-life of ^{224}Ra. In contrast, in a fully mixed water column, ^{224}Ra released from sediments is homogenously distributed and, thus, is detectable in the surface layers [see, for example, *Burt et al.*, 2013b]. Accordingly, model results are displayed as a mean ^{224}Ra distribution for the summer months of 2007 (June–August, Figure 8a) where seasonal stratification extends far south into the SNS, with the boundary between mixed and stratified water approximating the 30 m water depth isopleth. Furthermore, we show the mean ^{224}Ra distribution for the autumn months of 2007 (October–December, Figure 8b), when the fully mixed region of the SNS expands further north, with the boundary between mixed and stratified water approximately mirroring the 50 m water depth isopleth. Our cruise, in September 2011, coincided with numerous autumn storms, resulting in a

substantially mixed SNS (see stratification factor, Figure 3d), and thus, the observed surface ^{224}Ra distributions can be expected to be best represented by the autumn simulation (Figure 8b).

Little or no Ra is predicted in the NNS due to long-persisting seasonal and beyond seasonal stratification, higher water depths, and inflow of Atlantic water which is here considered to contain no Ra. Furthermore, model runs without a sediment source (Figure 8c) show the extent of the coastal signal into the North Sea. This result is consistent with the small relative contribution of coastal sources observed in the Ra mass balance and indicates that calculated values for Wadden Sea and riverine input are too small to explain the high activities and inventories observed in the CCW.

Quantitative analysis, illustrated in the Taylor diagram (Figure 8d), confirms the good agreement between observations and model results for the "mixed" SNS (Figure 8d). The autumn simulation shows a lower root-mean-square and a stronger correlation between the simulation and observations compared to the summer "stratified" simulation. The quality of the fit indicates that the calculated benthic flux terms obtained in our study are reasonable.

Given that seasonal variations in benthic Ra fluxes have not been reported previously, our assumption that the ^{224}Ra flux is constant over time is a reasonable one. Enhanced wind mixing in wintertime may induce more sediment-water column exchange via irrigation, but the magnitude of this increase is unclear. Unlike benthic oxygen, carbon and nutrients fluxes, which show significant seasonal variations in the North Sea [*Luff and Moll*, 2004], Ra efflux is not affected by seasonally varying deposition of organic material and therefore is not expected to exhibit substantial seasonal cycles.

We also assumed that the ^{224}Ra flux is invariant in space. Possibly an improved agreement between observed and simulated ^{224}Ra distributions can be achieved by resolving the spatial variability of the ^{224}Ra fluxes into the water column. As argued above, currently there does not appear to be a clear direct spatial/regional dependency of the ^{224}Ra fluxes, rather this dependency is mediated by the sediment typology (see Figure 6). Future studies dedicated to improved sediment sampling resolution could address this.

5. Conclusions

Throughout the North Sea, short-lived Ra is enriched in the water column due to interactions with the underlying sediments. Results from sediment incubations show considerable variation in benthic Ra efflux throughout the North Sea, attributable to differences in sediment characteristics such as porosity and grain size. Two independent water column-based approaches, Ra inventory and mass balance, yield benthic fluxes that are consistent and larger than both our incubation estimates, and those reported for most other regions. We attribute this to the turbulent conditions at the interface of permeable sandy sediments in the SNS, which lead to substantial irrigation, large amounts of sediment-water column exchange and, thus, large Ra fluxes. Using Ra flux estimates and pore water measurements, we calculate volume fluxes across the sediment-water interface, which are related to benthic A_T exchanges. Finally, results from the ECOSMO model runs further validate our estimated benthic fluxes while providing insight into seasonal variability of Ra distribution in the North Sea.

Sediment-water column exchange plays an important role in coastal biogeochemistry, and this study, along with previous ones, indicates that short-lived Ra is a useful tracer for quantifying rates of this exchange. This study represents the first large-scale study of short-lived radium in the North Sea and details a unique sampling strategy, including three-dimensional water column coverage as well as sediment sampling. This work should also provide motivation toward future use of Ra in both benthic-pelagic coupling studies and studies related to Wadden Sea impacts. Future North Sea sampling regimes would further this understanding of spatial and temporal variation in North Sea fluxes, which could lead to refined Ra modeling techniques. From a methodological standpoint, utilization of the recently developed Th/Ra disequilibrium method [*Cai et al*., 2014] in North Sea box core samples could lead to more precise estimates of benthic nutrient, oxygen, and carbon fluxes, as well as to a more in-depth understanding of the links between Ra and other important dissolved materials, such as alkalinity and carbon dioxide.

Appendix A: Data Table

Surface (5 m) Ra activities and a sampling summary for all 61 stations are provided in Table A1.

Table A1. Summary of Samples

Station	Latitude °N	Longitude °E	^{224}Ra (dpm 100 L^{-1})	^{223}Ra (dpm 100 L^{-1})	Near-Bottom Profile	Incubation	Pore Water Sampling
1	51.1	1.5	5.7	0.9			
2	51.6	2.0	5.3	0.4	x	x	
3	51.5	3.0	9.7	2.2			
4	52.0	3.5	10.9	1.2			
5	52.0	2.5	4.3	0.3			
6	52.6	2.5	4.8	0.5			
7	52.6	3.5	5.8	0.9	x	x	
8	52.6	4.0	8.7	0.7			
9	53.2	4.5	11.7	1.5			
10	53.2	3.5	6.1	1.0			
11	53.2	2.5	5.8	0.9	x	x	x
12	53.2	1.5	6.5	0.8			
13	53.8	0.5	5.0	0.6			
14	53.8	1.5	5.0	0.4			
15	53.8	2.8	7.5	0.9			
16	53.8	4.0	4.6	0.7			
17	53.8	5.3	7.6	0.8	x	x	x
18	53.8	6.5	10.4	1.8			
19	54.0	7.5	10.4	2.2			
20	54.4	8.1	14.4	1.6	x[a]	x	
21	54.4	7.5	6.0	1.0			
22	54.4	6.5	5.5	0.7			
23	54.4	5.2	4.6	0.9			
24	54.4	4.0	5.3	0.8			
25	54.4	3.0	4.5	0.6			
26	54.4	1.5	1.2	0.2			
27	54.4	0.5	0.7	0.0			
28	55.0	7.5	7.2	0.8			
29	55.0	6.5	4.5	0.9			
30	55.0	5.0	2.5	0.4	x	x	x
31	55.0	3.5	2.2	0.3			
32	55.0	2.0	3.4	0.1	x	x	x
33	55.0	0.5	0.5	0.0	x		
34	55.0	−0.5	0.2	0.0			
35	56.0	−1.5	0.9	0.1			
36	56.0	−0.5	0.0	0.0			
38	56.0	2.0	0.5	0.0	x	x	x
39	56.0	3.5	0.4	0.0			
40	56.0	5.0	0.7	0.0			
41	56.0	6.5	3.3	0.7			
42	56.0	7.5	7.4	0.7	x		x
43	57.0	7.5	5.1	0.3			
44	57.0	6.5	2.0	0.2			
45	57.0	5.3	0.0	0.0	x	x	x
46	57.0	3.8	0.3	0.0			
47	57.0	2.2	0.6	0.0			
48	57.0	0.9	0.1	0.0			
49	57.0	−0.5	0.5	0.0			
50	57.0	−1.5	0.8	0.0			
51	57.5	6.0	0.5	0.0			
52	57.5	7.5	0.8	0.1			
53	57.5	8.5	3.0	0.2			
59	58.0	4.2	0.5	0.0			
60	58.0	5.5	0.7	0.1			
61	58.0	8.5	0.9	0.0			
62	58.0	9.5	3.8	0.1	x	x	
63	58.0	10.4	2.8	0.1			
64	58.5	10.1	0.6	0.1			
65	58.5	9.5	0.3	0.0	x	x	

Table A1. (continued)

Station	Latitude °N	Longitude °E	^{224}Ra (dpm 100 L^{-1})	^{223}Ra (dpm 100 L^{-1})	Near-Bottom Profile	Incubation	Pore Water Sampling
66	58.2	8.5	1.9	0.4			
67	58.0	6.5	1.1	0.1			

[a]Two near-bottom samples instead of three.

Acknowledgments
We would like to acknowledge U. Braeckman, M. Hagens, L. Salt, and E. Jones along with the captain and crew of the R/V *Pelagia* for helping with sample collection and general cooperation with our fieldwork. In addition, we thank M. Rutgers Van-der Loeff for assistance with the data analysis. Finally, we thank both reviewers, whose detailed comments undoubtedly led to improvements in the manuscript. Financial support was provided by the POME exchange program (SIU, Norwegian Center for International Cooperation in Education), the Dutch Science Foundation (NWO, National Programme Sea and Coastal Research ZKO grant 839.10.500), the EU-FP7 SeasERA project SEAMAN and Killam Trusts. Data used are contained in the appendix of the manuscript.

References

Aller, R. C. (1980), Diagenetic processes near the sediment–water interface of Long Island Sound. I. Decomposition and nutrient element geochemistry (S, N, P), *Adv. Geophys.*, *22*, 235–348.

Barthel, K., U. Daewel, D. Pushpadas, C. Schrum, M. Årthun, and H. Wehde (2012), Resolving frontal structures: On the computational costs and pay-off using a less diffusive but more computational more expensive advection scheme, *Ocean Dyn.*, *62*, 1457–1470, doi:10.1007/s10236-012-0578-9.

Beck, M., O. Dellwig, G. Liebezeit, B. Schnetger, and H.-J. Brumsack (2008), Spatial and seasonal variations of sulphate, dissolved organic carbon, and nutrients in deep pore waters of intertidal flat sediments, *Estuarine Coastal Shelf Sci.*, *79*, 307–316.

Bozec, Y., H. Thomas, L.-S. Schiettecatte, A. V. Borges, K. Elkalay, and H. J. W. de Baar (2006), Assessment of the processes controlling seasonal variations of dissolved inorganic carbon in the North Sea, *Limnol. Oceanogr.*, *51*, 2746–2762.

Burt, W. J., H. Thomas, K. Fennel, and E. Horne (2013a), Sediment-water column fluxes of carbon, oxygen and nutrients in Bedford Basin, Nova Scotia, inferred from ^{224}Ra measurements, *Biogeosciences*, *10*, 53–66.

Burt, W. J., H. Thomas, and J.-P. Auclair (2013b), Short-lived radium isotopes on the Scotian Shelf: Unique distributions and tracers of cross-shelf CO_2 and nutrient transport, *Mar. Chem.*, *156*, 120–129.

Cai, P., X. Shi, W. S. Moore, and M. Dai (2012), Measurement of ^{224}Ra:^{228Th} disequilibrium in coastal sediments using a delayed coincidence counter, *Mar. Chem.*, *138-139*, 1–6.

Cai, P., X. Shi, W. S. Moore, S. Peng, G. Wang, and M. Dai (2014), ^{224}Ra:^{228}Th disequilibrium in coastal sediments: Implications for solute transfer across the sediment-water interface, *Geochim. Cosmochim. Acta*, *125*, 68–84.

Colbert, S. L., and D. E. Hammond (2008), Shoreline and seafloor fluxes of water and short-lived Ra isotopes to surface water of San Pedro Bay, CA, *Mar. Chem.*, *108*, 1–17.

Daewel, U., and C. Schrum (2013), Simulating long-term dynamics of the coupled North Sea and Baltic Sea ecosystem with ECOSMO II: Model description and validation, *J. Mar. Syst.*, *119-120*, 30–49.

Dauwe, B., P. M. J. Herman, and C. H. R. Heip (1998), Community structure and bioturbation potential of macrofauna at four North Sea stations with contrasting food supply, *Mar. Ecol. Prog. Ser.*, *173*, 67–83.

de Haas, H., T. C. E. van Weering, and H. de Stiger (2002), Organic carbon in shelf seas: sinks or sources, processes and products, *Cont. Shelf Res.*, *22*, 691–717.

Hancock, G. J., I. T. Webster, P. W. Ford, and W. S. Moore (2000), Using Ra isotopes to examine transport processes controlling benthic fluxes into a shallow estuarine lagoon, *Geochim. Cosmochim. Acta*, *64*, 3685–3699.

Hancock, G. J., I. T. Webster, and T. C. Stieglitz (2006), Horizontal mixing of Great Barrier Reef waters: Offshore diffusivity determined from radium isotope distribution, *J. Geophys. Res.*, *111*, C12019, doi:10.1029/2006JC003608.

Holt, J. T., and I. D. James (1999), A simulation of the southern North Sea in comparison with measurements from the North Sea Project. Part 2—Suspended particulate matter, *Cont. Shelf Res.*, *19*, 1617–1642.

Hoppema, J. M. J. (1990), The distribution and seasonal variation of alkalinity in the Southern Bight of the North Sea and in the Western Wadden Sea, *Neth. J. Sea Res.*, *26*, 11–23.

Huettel, M., and G. Gust (1992), Solute release mechanisms from confined sediment cores in stirred benthic chambers and flume flows, *Mar. Ecol. Prog. Ser.*, *82*, 187–197.

Jahnke, R. A., J. R. Nelson, R. L. Marinelli, and J. E. Eckman (2000), Benthic flux of biogenic elements on the Southwestern US continental shelf: Influence of pore water advective transport and benthic microalgae, *Cont. Shelf Res.*, *20*, 109–127.

Jahnke, R., M. Richards, J. Nelson, C. Robertson, A. Rao, and D. Jahnke (2005), Organic matter remineralization and porewater exchange rates in permeable South Atlantic Bight continental shelf sediments, *Cont. Shelf Res.*, *25*, 1433–1452.

Janssen, F., P. Faerber, M. Huettel, V. Meyer, and U. Witte (2005a), Pore-water advection and solute fluxes in permeable marine sediments (I): Calibration and performance of the novel benthic chamber system *Sandy*, *Limnol. Oceanogr.*, *50*, 768–778.

Janssen, F., M. Huettel, and U. Witte (2005b), Pore-water advection and solute fluxes in permeable marine sediments (II): Benthic respiration at three sandy sites with different permeabilities (German Bight, North Sea), *Limnol. Oceanogr.*, *50*, 779–792.

Kelly, R. P., and S. B. Moran (2002), Seasonal changes in groundwater input to a well-mixed estuary estimated using radium isotopes and implications for coastal nutrients budgets, *Limnol. Oceanogr.*, *47*, 1796–1807.

Lee, A. J. (1980), North Sea: Physical Oceanography, in *The North-West European Shelf Seas the Seabed and the Sea in Motion II. Physical and Chemical Oceanography*, *Elsevier Oceanogr. Ser.*, vol. 24B, edited by F. T. Banner, M. B. Collins, and K. S. Massie, pp. 467–493, Elsevier, Amsterdam, Netherlands.

Lohse, L., E. H. G. Epping, W. Helder, and W. van Raaphorst (1996), Oxygen pore water profiles in continental shelf sediments of the North Sea: Turbulent versus molecular diffusion, *Mar. Ecol. Prog. Ser.*, *145*, 63–75.

Luff, R., and A. Moll (2004), Seasonal dynamics of the North Sea sediments using a three-dimensional coupled sediment-water model system, *Cont. Shelf Res.*, *24*, 1099–1127.

Moore, W. S. (2007), Seasonal distribution and flux of radium isotopes on the southeastern U.S. continental shelf, *J. Geophys. Res.*, *112*, C10013, doi:10.1029/2007JC004199.

Moore, W. S., and R. Arnold (1996), Measurement of ^{223}Ra and ^{224}Ra in coastal waters using a delayed coincidence counter, *J. Geophys. Res.*, *101*, 1321–1329, doi:10.1029/95JC03139.

Moore, W. S., J. O. Blanton, and S. B. Joye (2006), Estimates of flushing times, submarine groundwater discharge, and nutrient fluxes to Okatee Estuary, South Carolina, *J. Geophys. Res.*, *111*, C09006, doi:10.1029/2005JC003041.

Moore, W. S., M. Beck, T. Riedel, M. Rutgers van der Loeff, O. Dellwig, T. J. Shaw, B. Schnetger, and H.-J. Brumsack (2011), Radium-based pore water fluxes of silica, alkalinity, manganese, DOC, and uranium: A decade of studies in the German Wadden Sea, *Geochim. Cosmochim. Acta*, *75*, 6535–6555.

Omar, A. M., A. Olsen, T. Johannessen, M. Hoppema, H. Thomas, and A. V. Borges (2010), Spatiotemporal variations of fCO_2 in the North Sea, *Ocean Sci.*, *6*, 77–89.

Pätsch, J., and W. Kühn (2008), Nitrogen and carbon cycling in the North Sea and exchange with the North Atlantic-A model study. Part 1. Nitrogen budget and fluxes, *Cont. Shelf Res.*, *28*, 767–787.

Pätsch, J., and H.-J. Lenhart (2011), Daily loads of nutrients, total alkalinity, dissolved inorganic carbon and dissolved organic carbon of the European continental rivers for the years 1977–2009. [Available at http://www.ifm.zmaw.de/research/theoretical-oceanography/models-and-data/ersem-and-ecoham/.]

Precht, E., and M. Huettel (2003), Advective pore-water exchange driven by surface gravity waves and its ecological implications, *Limnol. Oceanogr.*, *48*, 1674–1684.

Rusch, A., and M. Huettel (2000), Advective particle transport into permeable sediments-evidence from experiments in an intertidal sandflat, *Limnol. Oceanogr.*, *45*, 525–533.

Rutgers van der Loeff, M. M. (1980), Nutrients in the interstitial waters of the Southern Bight of the North Sea, *Neth. J. Sea Res.*, *14*, 144–171.

Santschi, P. H., R. F. Anderson, M. Q. Fleisher, and W. Bowles (1991), Measurements of diffusive sublayer thicknesses in the ocean by alabaster dissolution, and their implications for the measurements of benthic fluxes, *J. Geophys. Res.*, *96*, 10,641–10,657, doi:10.1029/91JC00488.

Schmidt, C., C. Hanfland, P. Regnier, P. Van Cappellen, M. Schlüter, U. Knauthe, I. Stimac, and W. Geibert (2010), ^{228}Ra, ^{226}Ra, ^{224}Ra and ^{223}Ra in potential sources and sinks of land-derived material in the German Bight of the North Sea: Implications for the use of radium as a tracer, *Geo-Mar Lett.*, *31*, 259–269, doi:10.1007/s00367-011-0231-5.

Schrum, C., I. Alekseeva, and M. St. John (2006), Development of a coupled physical-biological ecosystem model ECOSMO Part 1: Model description and validation for the North Sea, *J. Mar. Sys.*, *61*, 79–99, doi:10.1016/j.jmarsys.2006.01.005.

Shaw, T. J. (2003), Methods and models for estimating advective pore water exchange in tidal flats, *Ber. Forschungsz. Terramare*, *12* 103–104.

Slomp, C. P., J. F. P. Malschaert, L. Lohse, and W. Van Raaphorst (1997), Iron and manganese cycling in different sedimentary environments on the North Sea continental margin, *Cont. Shelf Res.*, *17*, 1083–1117.

Taylor, K. E. (2001), Summarizing multiple aspects of model performance in a single diagram, *J. Geophys. Res.*, *106*, 7183–7192, doi:10.1029/2000JD900719.

Tengberg, A., et al. (2005), Intercalibration of benthic flux chambers—II. Hydrodynamic characterization and flux comparisons of 14 different designs, *Mar. Chem.*, *94*, 147–173.

Thomas, H., L.-S. Schiettecatte, K. Suykens, Y. J. W. Kone, E. H. Shadwick, A. E. F. Prowe, Y. Bozec, H. J. W. de Baar, and A. V. Borges (2009), Enhanced ocean storage from anaerobic alkalinity generation in coastal sediments, *Biogeosciences*, *6*, 267–274.

van Duyl, F. C., and A. J. Kop (1994), Bacterial production in North Sea sediments: Clues to seasonal and spatial variations, *Mar. Biol.*, *120*, 323–337.

van Raaphorst, W., H. T. Kloosterhuis, A. Cramer, and K. J. M. Bakker (1990), Nutrient early diagenesis in the sandy sediments of the Dogger Bank area, North Sea: Pore water results, *Neth. J. Sea Res.*, *26*, 25–52.

van Raaphorst, W., H. T. Kloosterhuis, E. M. Berghuis, A. J. M. Gieles, J. F. P. Malschaert, and G. J. van Noort (1992), Nitrogen cycling in the two types of sediments of the Southern North Sea (Frisian Front, Broad Fourteens): Field data and mesocosm results, *Neth. J. Sea Res.*, *28*, 292–316.

Weisner, M. G., B. Haake, and H. Wirth (1990), Organic facies of surface sediments in the North Sea, *Org. Geochem.*, *15*, 419–432.

Winde, V., M. E. Böttcher, P. Escher, P. Böning, M. Beck, G. Liebezeit, and B. Schneider (2014), Tidal and spatial variations of DI^{13}C and aquatic chemistry in a temperate tidal basin during winter time, *J. Mar. Syst.*, *129*, 396–404.